Surface effects in ferrimagnetic TbFe rare-earth–transition-metal thin films and nanoparticles

Paweł Sobieszczyk and Michal Krupinski*
Institute of Nuclear Physics Polish Academy of Sciences, Radzikowskiego 152, Kraków 31-342, Poland

(Received 19 April 2023; revised 11 December 2023; accepted 14 December 2023; published 10 January 2024)

Alterations of magnetic properties associated with a large surface-to-volume ratio are of great importance for all magnetic nanosystems. In particular, amorphous rare-earth–transition-metal thin films with a thickness of 10 nm or less demonstrate modified $M(T)$ characteristics and magnetization switching behavior in comparison with their bulk counterparts. Understanding and experimentally identifying which particular surface phenomenon is responsible for this behavior are challenges due to the variety of possible overlapping contributions and effects. In this paper, we report on a study of surface magnetism in amorphous ferrimagnetic TbFe thin films and nanoparticles with varying diameters. We demonstrate how the reduction of the average number of surface neighbors, preferential oxidation, and chemical segregation can change compensation and Curie temperatures as well as magnetic reversal characteristics of the alloy. Our results indicate that the preferential oxidation plays a leading role, whereas reduction of the average number of neighbors and chemical segregation are found to be the second most important factors.

DOI: 10.1103/PhysRevB.109.024412

I. INTRODUCTION

Thin films and nanostructures of the rare-earth–3*d*-transition-metal (RE-TM) alloys are the subject of many fundamental and applied studies. Especially Tb-Fe, Gd-Fe, Tb-Co, and Gd-Co amorphous systems are of great interest due to their unique ferrimagnetic properties and the simultaneous occurrence of many interesting phenomena such as perpendicular magnetic anisotropy [1], ultrafast magnetization switching by current pulses [2], magnetostriction [3], all-optical switching [4], domains without domain walls [5], and a compensation temperature T_m, where the net magnetization is zero. The abovementioned properties can be engineered and adjusted to the requirements by RE content [6,7], surface morphology [8,9], modifications of local atomic order [10], or thin film thickness [11]. The latter parameter affects in particular the compensation point and remanent magnetization in structures thinner than 20–30 nm [6,12]. For instance, Hebler *et al.* [12] showed that increasing $Tb_{25}Fe_{75}$ film thickness from 9 to 28 nm results in the shift of the compensation temperature from 150 to 370 K, while for thicker layers no significant effect was observed. Similar dependencies have been reported by other authors for other RE-TM alloys [6,13], which indicates the presence of surface effects that are noticeable only for sufficiently thin layers.

The origin of this effect is not well understood, and several contributions are considered to explain it. One possibility is a nonhomogeneous distribution of the rare earth atoms along the film thickness which may be induced by selective resputtering during the growth process [14,15], by a chemical segregation process [2,16–19], or by interaction with seed and capping layers [18,20]. In addition, selective oxidation of rare earth atoms can occur near the surface due to diffusion of oxygen through thin protective layers or out of the substrate [20–23]. While some authors evidenced the above reasons as a source of a nonhomogeneous rare earth content distribution within the film depth [20,24,25], others argue [12,26] that the composition changes are insignificant and cannot account for the variation in magnetic properties. Therefore other explanations have also been proposed. One of the possibilities is a contribution of stress-induced effects, which can play a decisive role in the sub-10-nm thickness range [12,27]. On the other hand, Ma *et al.* [26] demonstrated that the surface effects may result from a surface region of about 5 nm where a different alloy amorphous phase forms. The formation of the additional phase is associated with changes in the short-range order of the RE-TM alloy, which strongly influences its structure and magnetism. Another possibility proposed by Hebler *et al.* [12] is an alteration of the fanning cone for RE atomic moments related to growth-induced variations in the short-range order. With decreasing film thickness, the total exchange energy can decrease, which causes a widening of RE fanning cone angle and a decreasing contribution of the RE sublattice magnetization to the total sample magnetization. This, however, contradicts the result of the paper by Ruckert *et al.* [28], who showed that the fanning cone does not vary strongly with film thickness.

The variety of possible overlapping surface effects that may affect the magnetic properties of RE-TM alloys significantly hinders systematic experimental research into these magnetic properties. On the basis of current experimental data, it is difficult to clearly state which of the surface effects plays a leading role and which has negligible importance. Progress in exploring this issue may, however, be achieved by employing computational tools. For this purpose, we built an atomistic spin model validated by comparison with experimental results, and we analyzed the influence of individual

*michal.krupinski@ifj.edu.pl

surface effects using an atomistic simulation approach that allows us to separate the individual contributions and determine their impact on the compensation temperature, remanent magnetization, and hysteresis loop behavior. We performed the calculations for the representative TbFe system in the form of thin films as well as spherical nanoparticles, where the surface-to-volume ratio is bigger than in thin films with a thickness corresponding to the diameter of the nanoparticle. Such an approach allows us not only to track the magnetic changes originating from the surface but also to explore the prospects of RE-TM nanoparticles, whose properties are so far poorly researched due to the difficulties in the experimental fabrication of this type of system [29,30].

II. METHODS

Atomistic calculations were performed using VAMPIRE software [31]. The TbFe alloy with 25 at. % of terbium was modeled as two ferromagnetic sublattices coupled antiferromagnetically. In order to mimic the disordered or amorphous phase, the sites in an fcc lattice (unit cell size 3.5 Å) were randomly occupied by Tb or Fe atoms. The distance between the magnetic ions does not appear explicitly in the Hamiltonian, but is included in the adopted values of the exchange coupling constants. They are stated per link and do not take into account the number of neighbors of each species [32]. All the reference results for bulk systems have been obtained for a sample volume size of $20 \times 20 \times 20$ nm^3 with periodic boundary conditions in the x, y, and z directions. In the case of nanoparticles, single objects were simulated without boundary conditions, while the periodic boundary conditions in the x and y directions were applied for thin films. The magnetization dynamics for the ith atom is governed by the stochastic form of the Landau-Lifshitz-Gilbert equation with Langevin dynamics

$$\frac{d\mathbf{S}_i}{dt} = -\frac{\gamma_i}{\left(1+\lambda_i{}^2\right)\mu_i}\left(\mathbf{S}_i \times \mathbf{H}_i^{\text{eff}}\right) + \lambda_i \mathbf{S}_i \times \left[\mathbf{S}_i \times \mathbf{H}_i^{\text{eff}}\right], \quad (1)$$

where $\mathbf{S}_i$ is a normalized spin vector, μ_i is an atomistic spin moment on the given site, γ_i is a gyromagnetic ratio, and λ_i is a Gilbert damping constant. For the sake of simplicity, γ_i was the same for both sublattices.

The effective field is defined as $\mathbf{H}_i^{\text{eff}} = \eta_i(t) - \frac{\partial \mathcal{H}_i}{\partial \mathbf{S}_i}$ and acts on each atomic moment. A stochastic term $\eta_i(t)$ represents thermal fluctuations at given temperature T and is considered as white noise, uncorrelated in space and time [33].

$$\langle \eta_i(t)\eta_i(t')\rangle = \frac{2\lambda_i k_B T \mu_i}{\gamma_i}\delta_{ij}\delta_{\alpha\beta}\delta(t-t'). \quad (2)$$

The Hamiltonian of the system is described as follows:

$$\mathcal{H} = -\frac{1}{2}\sum_{\langle ij\rangle} J_{ij}\mathbf{S}_i \cdot \mathbf{S}_j - \sum_{i=1}^{N} K_i^u (\mathbf{S}_i \cdot \mathbf{n}_i)^2 - \sum_{i=1}^{N} \mu_i \mathbf{B}^{\text{ext}} \cdot \mathbf{S}_i, \quad (3)$$

where J_{ij} is the nearest-neighbor exchange constant between sites i and j and depends on the sublattice. The adopted values of the exchange coupling constants were $J^{\text{Fe-Fe}} = 2.75 \times 10^{-21}$ J, $J^{\text{Tb-Tb}} = 1.25 \times 10^{-21}$ J, and $J^{\text{Tb-Fe}} = -1.65 \times 10^{-21}$ J, and these values were determined from previous studies supported by experiment [10]. The average magnetic moments per atom were $\mu_{\text{Fe}} = 2.218\ \mu_B$ and $\mu_{\text{Tb}} = 9.0\ \mu_B$ for iron and terbium, respectively [10]. K_i^u is a uniaxial anisotropy constant with a vector n_i^z, and $\mathbf{B}^{\text{ext}}$ is an external magnetic field. For simplicity, we assume that the uniaxial anisotropy is the same for both sublattices, and it is taken as $K_u = 8 \times 10^{-24}$ J/atom at 0 K. An additional linear dependence of the anisotropy constant on temperature has been taken into account according to Hansen *et al.* [34]. Magnetization saturation as a function of temperature was calculated using the Monte Carlo method with a time step of 10^{-15} s. We considered that the system reaches magnetic equilibrium at the given temperature after 10^5 integration steps, which corresponds to 0.1 ns [35]. For the hysteresis loops, the Huen method was used with a total observation time of 1.5×10^5 steps [36]. In each case, noninteracting nanoparticles were simulated. The magnetostatic energy within one particle was three orders of magnitude lower than the exchange interaction energy and therefore was considered as insignificant.

The atomistic simulations were supported by mean field approximation (MFA) calculations to obtain exchange constants for a given concentration of terbium and also to compare the atomistic results with a simple MFA model for two sublattices [32]. In this approach, the effective field can be divided into two parts representing two sublattices:

$$\begin{aligned}\mu_{\text{Tb}}\mathbf{H}_{\text{Tb}}^{\text{MFA}} &= \mu_{\text{Tb}}\mathbf{H'}_{\text{Tb}} + xJ_0^{\text{Tb-Tb}}\boldsymbol{s}_{\text{Tb}} + qJ_0^{\text{Tb-Fe}}\boldsymbol{s}_{\text{Fe}}\\ \mu_{\text{Fe}}\mathbf{H}_{\text{Fe}}^{\text{MFA}} &= \mu_{\text{Fe}}\mathbf{H'}_{\text{Fe}} + qJ_0^{\text{Fe-Fe}}\boldsymbol{s}_{\text{Fe}} + xJ_0^{\text{Fe-Tb}}\boldsymbol{s}_{\text{Tb}},\end{aligned} \quad (4)$$

where $J_0 = \epsilon n J_{ij}$, n is the average coordination number, $\epsilon = 0.79$ for an fcc lattice [37], x is the concentration of terbium, and $q = 1 - x$. $\mathbf{H}' = \mathbf{H}^{\text{ext}} + \mathbf{H}_i^{\text{anis}}$, where $\mathbf{H}^{\text{ext}}$ is the external magnetic field and $\mathbf{H}_i^{\text{anis}} = 2(K_i^u/\mu_i)s_{i,z}$ is the anisotropy field acting on each spin. Finding an equilibrium solution of the system of two sublattices leads to coupled Curie-Weiss equations:

$$\boldsymbol{s}_{\text{Tb}} = L(\xi_{\text{Tb}})\frac{\boldsymbol{\xi}_{\text{Tb}}}{\xi_{\text{Tb}}}, \quad \boldsymbol{s}_{\text{Fe}} = L(\xi_{\text{Fe}})\frac{\boldsymbol{\xi}_{\text{Fe}}}{\xi_{\text{Fe}}}, \quad (5)$$

where $L(\xi_{\text{Tb}})$ is a Langevin function and $\xi_i = \mu_i \mathbf{H}_i^{\text{MFA}}/k_B T$. Then, the total magnetization of the equilibrium system can be derived from the self-consistent solution and takes the form

$$\mathbf{M} = \mu_{\text{Fe}} q \mathbf{s}_{\text{equil,Fe}} - \mu_{\text{Tb}} x \mathbf{s}_{\text{equil,Tb}}. \quad (6)$$

III. RESULTS AND DISCUSSION

A. Reduction of the average number of neighbors

Representative results of atomistic simulations for a spherical nanoparticle of composition $Tb_{25}Fe_{75}$ and a diameter of 5 nm are shown in Fig. 1. The nanoparticle exhibits spontaneous magnetization in the direction determined by the anisotropy of the system. The anisotropy direction and energy are set at the stage of material production and are most often related to the ordering of atomic pairs or alterations in the local structure of the alloy [15,38]. Here, the main axis of anisotropy has been adopted along the z axis, resulting in a net magnetization close to that direction. The magnetic sublattices of terbium and iron show a distribution of magnetic

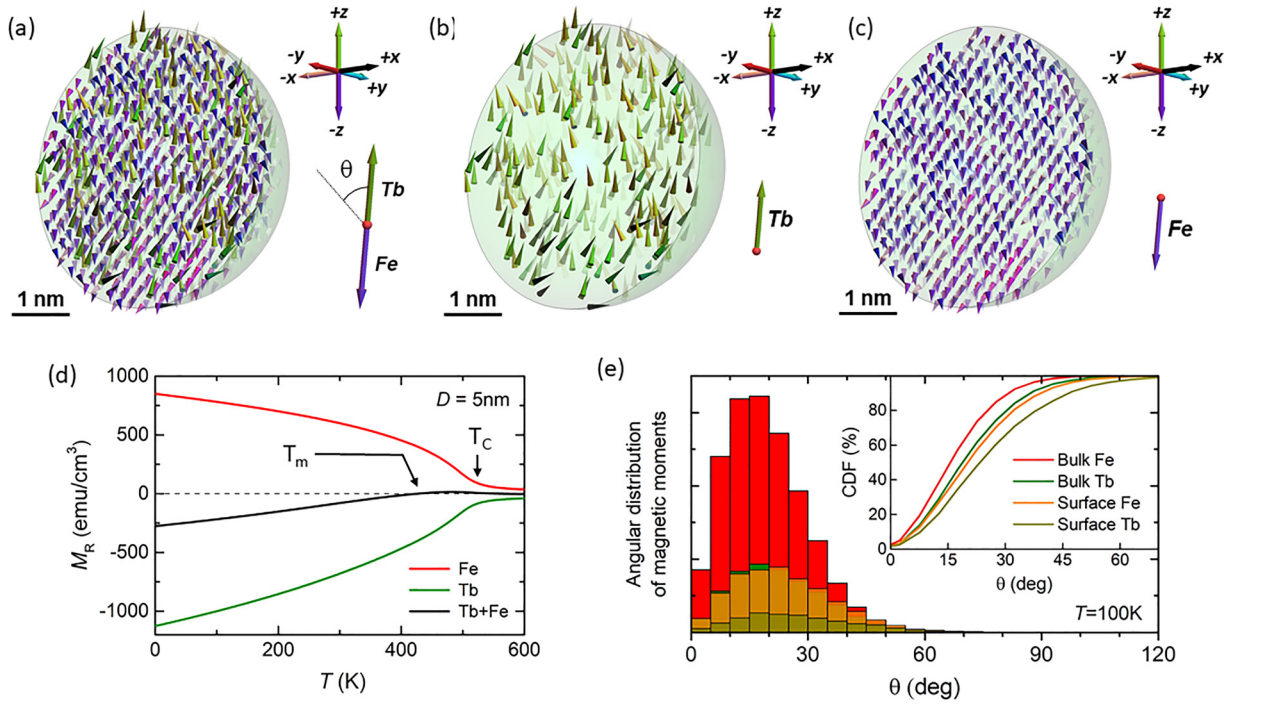

FIG. 1. (a) Visualization of magnetic moments at the cross section of a nanoparticle with a diameter of 5 nm at temperature 100 K. Terbium moments are marked with a green color scale, while iron moments are marked with a purple color scale. (b) and (c) The magnetic moments establishing terbium and iron sublattices, respectively. (d) Remanent magnetization vs temperature for iron (red) and terbium (green) sublattices together with net magnetic moment of the whole nanoparticle (black). (e) Angular distribution of magnetic moments for surface and bulk iron and terbium atoms. The inset presents the cumulative distribution function for the corresponding distributions. θ is the angle between the direction of a particular magnetic moment and the resultant magnetization of a nanoparticle.

moments [Figs. 1(b) and 1(c)], which is commonly designated as the "fanning cone" behavior observed in RE-TM systems [39,40]. The widths of these distributions change with temperature, which results in the $M_R(T)$ relationship showing a compensation temperature $T_m = 425$ K when the resultant magnetic moments of the sublattices cancel each other [Fig. 1(d)]. For a sufficiently high temperature, the spread of magnetic moments is so large that the spontaneous magnetization disappears and the material reaches the Curie temperature $T_C \approx 530$ K.

The magnetic moments located on Fe and Tb atoms can be divided into two subgroups: (i) surface moments with number of neighbors less than 12, which corresponds to a distance of less than 0.35 nm from the surface, and (ii) those located in the center of the nanoparticle at a distance of more than 0.35 nm from the surface designated as bulk moments. The angular distributions of these moments around the resultant magnetization direction of the particle are shown in Fig. 1(e). In all cases they follow the Boltzmann distribution, which is characteristic for thermally activated ensembles of spins with anisotropy [31]. Although the histograms for the bulk and surface magnetic moments appear to be similar, the cumulative distribution function (CDF) reveals significant differences between them. The surface moments have wider distributions with the maximum shifted towards larger angles by about 5°. This is caused by stronger thermal excitations of the surface magnetic moments that are less coupled to the lattice due to the smaller number of neighbors and therefore have less resultant exchange energy. A more detailed analysis of this phenomenon is shown in Fig. 2, where the angular distributions as a function of temperature for the bulk and surface magnetic moments in a 5-nm spherical nanoparticle are presented. From the cumulative distribution functions [Figs. 2(e)–2(h)], one can calculate the median tilting angle of the moments for a particular sublattice and temperature by determining the angle for which CFD = 50% (collected in Table I). For all temperatures, the median tilting angle is smaller for Fe than for Tb due to stronger interatomic Fe coupling in comparison with Tb moments exhibiting a weaker exchange coupling expressed through $J_{\text{Fe-Fe}} > J_{\text{Tb-Tb}}$. For bulk Fe moments, the angular distribution in thick films of amorphous TbFe alloys was directly measured using Mössbauer spectroscopy by Ruckert *et al.*, who determined the typical fanning cone angle to be about 30° [28], which agrees well with our calculations for 300 K. On the other hand, the average fanning cone angle of the bulk Tb moments

TABLE I. Median tilting angle (in degrees) for bulk and surface moments in Fe and Tb sublattices calculated for different temperatures.

	5 K	100 K	300 K	400 K
Fe bulk	3	15	33	43
Fe surface	4.5	20	41	57
Tb bulk	4	19	38	52
Tb surface	5	23	52	65

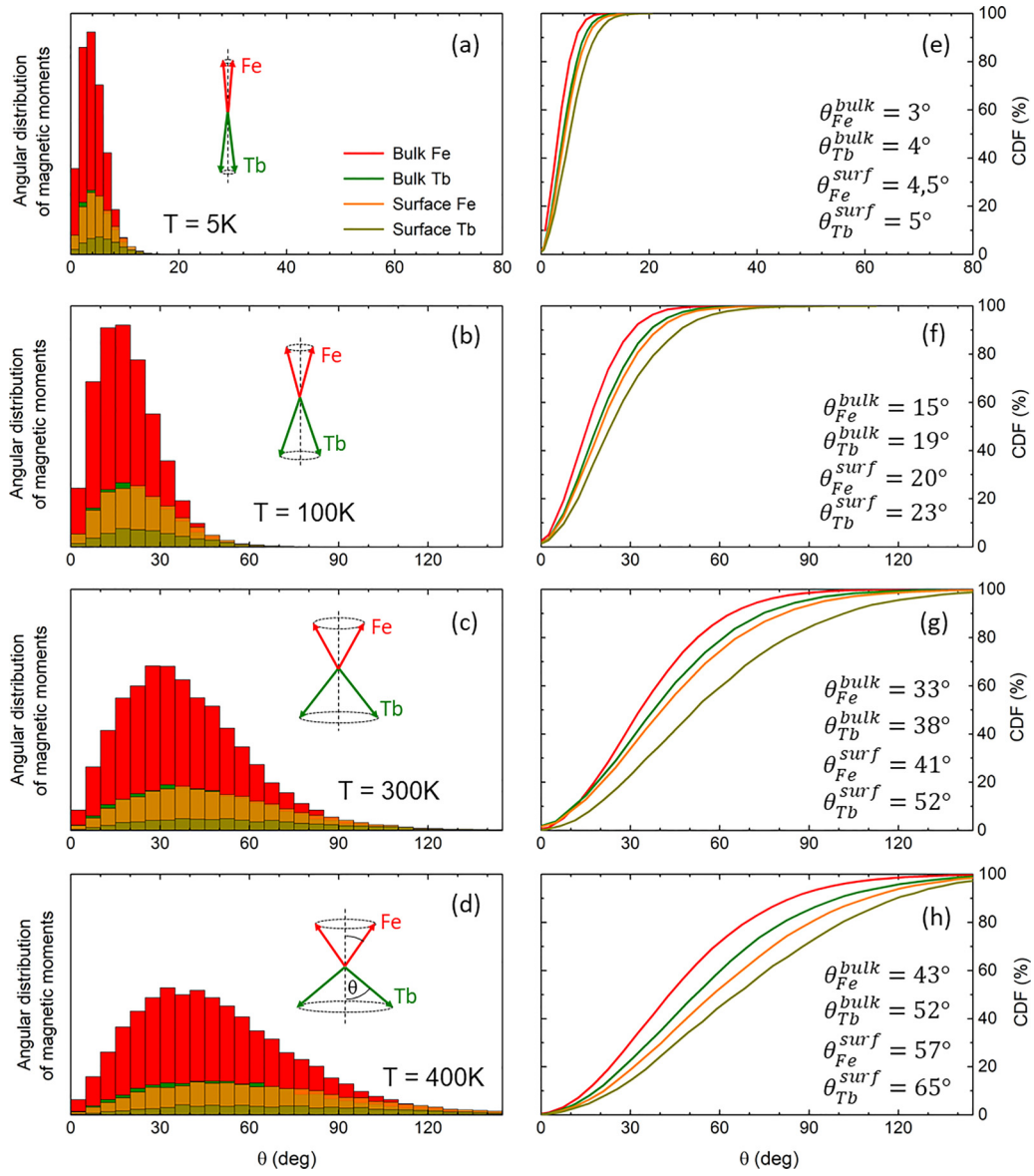

FIG. 2. (a)–(d) Angular distributions of magnetic moments for Tb and Fe sublattices calculated for a 5-nm spherical nanoparticle at various values of temperature. Contributions from surface and bulk magnetic moments are distinguished by different colors. (e)–(h) Cumulative distribution functions (CDFs) corresponding to the distributions of magnetic moments for a particular temperature. Note that the horizontal scale for the graphs in (a) and (e) is different from that for the other graphs.

can be experimentally estimated using $M(H)$ measurements in the high-magnetic-field regime supported by a macrospin simplification. Schubert established its value to be about $40^\circ \pm 5^\circ$ at room temperature for TbFe alloy film with 25 at. % Tb [41], which is bigger than the angle value of the bulk Fe magnetic moments and stays in reasonable agreement with simulation results presented here. The average widths of the orientational moment distributions are determined by the anisotropy constant and exchange coupling strength. Both of these quantities are altered on the surface of the nanoparticle by a different short-range order and a decrease in the number of nearest neighbors. In consequence, surface moments are more susceptible to thermal excitations, which is visible as a broadening of their angular distributions. The higher the temperature, the more pronounced these changes are, and for 400 K the broadening is 15° and 13° for Fe and Tb moments, respectively. The same effect can be observed for thin films, as shown in the Supplemental Material, Fig. S1 [42], where similar values of average fanning cone angles were found for a layer with thickness of 5 nm. In this case, however, the orientational distributions for surface and bulk moments have different contributions due to different geometry and smaller surface-to-volume ratio in comparison with nanoparticles.

Since the magnetic properties of RE-TM alloys are determined by the intrinsic configuration of the magnetic sublattice moments, the changes in the angular distributions influence the temperature behavior of the alloy and particularly its compensation point and Curie temperature. This allows different magnetic properties of the nanoparticles to be obtained despite there being the same alloy stoichiometry. Such a possibility is shown in Fig. 3, where the remanent magnetization vs temperature for nanoparticles with diameters from 2 to 12 nm

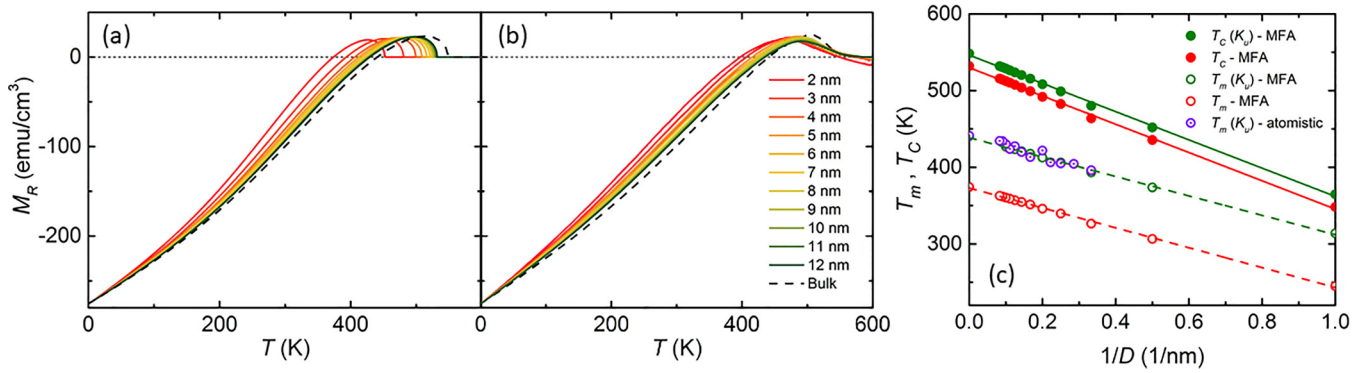

FIG. 3. Remanent magnetization vs temperature for TbFe nanoparticles calculated using (a) the mean field approximation and (b) the atomistic approach. The nanoparticle diameter varies in the range 2–12 nm. (c) Compensation and Curie temperatures determined on the basis of the mean field approximation and atomistic simulations as a function of reciprocal diameter. For MFA models, two cases were considered: without magnetic anisotropy (red points) and with anisotropy (green points). The anisotropy has always been taken into account in the case of the atomistic approach.

is presented in comparison with the result for bulk alloy. The curves were calculated using the mean field approximation [Fig. 3(a)] and the atomistic approach [Fig. 3(b)]. The average coordination number as a function of the nanoparticle diameter used in the mean field approximation is shown in the Supplemental Material, Fig. S2 [42]. Qualitatively similar results were obtained using the two methods, and the observed differences are due to the fact that the MFA model takes into account only the average exchange interaction for each magnetic sublattice, while the atomistic simulation considers the local variations of the neighbor configuration for each atom. The difference in the compensation point between the smallest particles and the bulk alloy reaches 70 K, and the same changes are observed for the Curie temperature [Fig. 3(c)]. Both temperatures scale linearly with the reciprocal of the particle diameter, and the approximation of the linear fits in Fig. 3(c) shows that T_m and T_C reach 0 K for diameters comparable to the distance between atoms, i.e., 0.35 nm. The observed linear scaling with $1/D$ corresponds to the behavior of the surface-area-to-volume ratio for spherical objects. The same type of dependence is present also for thin layers, where T_m scales linearly with the reciprocal of layer thickness $1/t$, as shown in the Supplemental Material, Fig. S3 [42]. In this case, however, the slope for the temperature trend T_m is smaller due to the different geometry of the system.

The influence of the surface effect is also visible in the $M(H)$ curves presented in Fig. 4, where the time-averaged (0.15 ns at each step) z-axis projection of the resultant moment of the nanoparticle is presented, with the external magnetic field directed also along the z axis. A greater share of surface atoms, and thus a greater spatial distribution of magnetic moments, makes magnetization switching easier to start through the spontaneous rotation of the weakly coupled moments on the surface. This is manifested by a decrease in the coercivity values compared with the bulk. At low temperatures, the coercivity reduction reaches about 20% for a nanoparticle with a diameter of 5 nm. At higher temperatures, an additional decrease of remanence and hysteresis loop squareness is visible. This can be interpreted as the onset of a superparamagnetic effect, where thermal fluctuations are responsible for the quick changes in the total magnetic moment direction. The predicted changes in hysteresis loop behavior, as well as shifts in T_m and T_C, indicate that surface effects related to the reduction of the average number of neighbors should be easily observable in RE-TM nanosystems and can be used to tune the compensation temperature; however, they are too small and cannot alone explain the large changes in compensation temperature observed in thin metal layers as a function of their thickness [12].

B. Preferential surface oxidation

Rare earth elements oxidize readily due to their small electronegativity. For this reason, thin layers of RE-TM alloys and nanoparticles are often protected by covering them with a few nanometers of a noble metal such as Pt or Ta. However, recent research has shown that despite the protective layers, oxygen can diffuse in a small amount into the material [2,20,22,23]; therefore a preferential oxidation is expected since rare elements have a greater tendency to bond with oxygen than transition metals do. Such a process has been examined by Bergeard *et al.* [23], who determined the structural and chem-

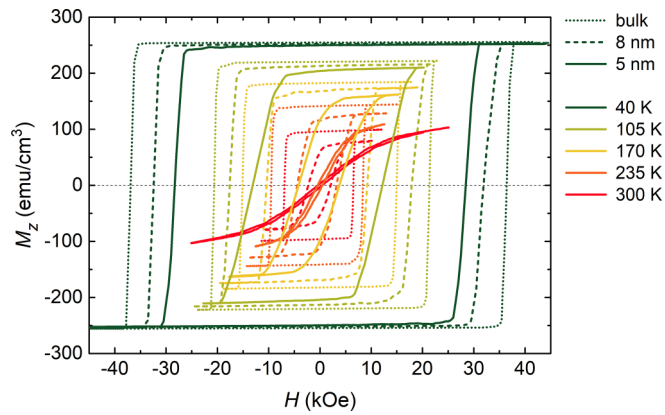

FIG. 4. $M_z(H)$ loops at various temperatures for the $Tb_{25}Fe_{75}$ alloy in the form of nanoparticles with diameters of 5 nm (solid curves) and 8 nm (dashed curves) and for the bulk (dotted curves). The magnetic field was applied in the direction of the easy axis of magnetization.

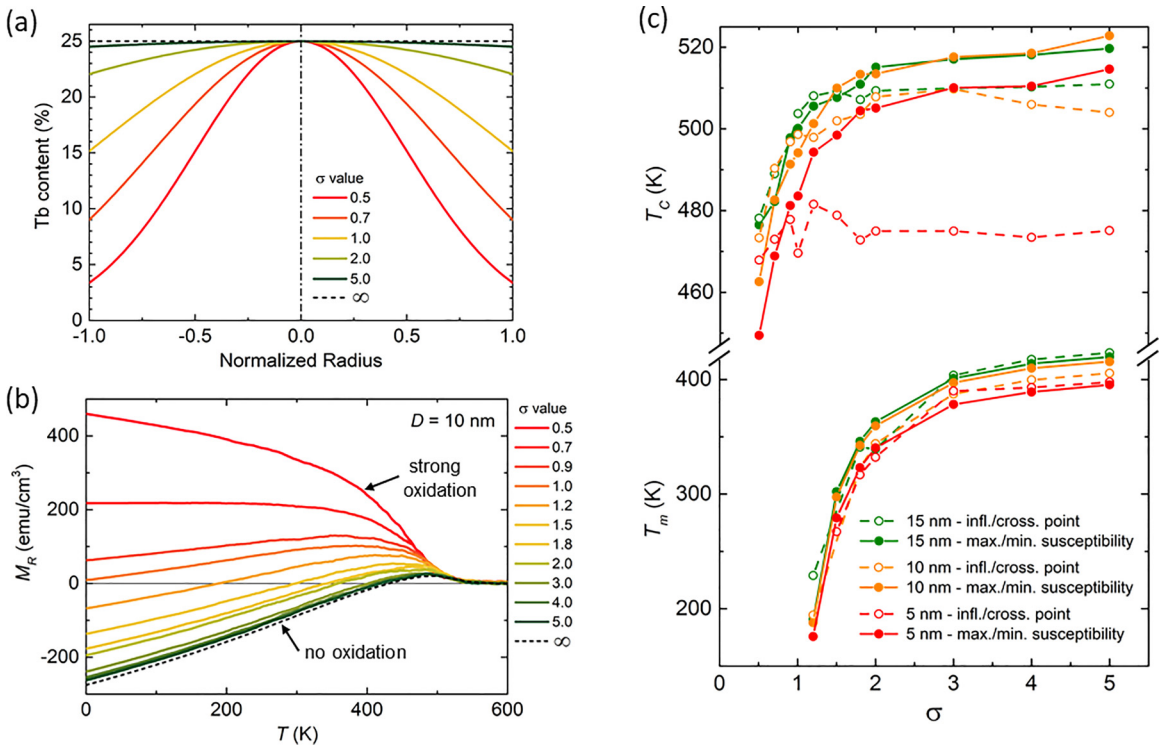

FIG. 5. (a) Distribution of Tb content in a nanoparticle as a function of distance from its center. The width of the distribution is expressed in the normalized radius of the nanoparticle. The infinite sigma value corresponds to a homogeneous concentration distribution throughout the volume of the nanoparticle. (b) Remanent magnetization vs temperature for 10-nm nanoparticles with various distributions of terbium content. (c) Upper part: Curie temperatures determined for nanoparticles of three different sizes using two methods, namely the maximum of the susceptibility (solid circles) and the inflection point of the $M(T)$ curve (open circles). Lower part: compensation temperatures determined for 5-, 10-, and 15-nm nanoparticles using the minimum of the susceptibility (solid circles) and the intercept of the $M(T)$ curve with the axis $M_R = 0$ (open circles). Note the different scales for T_C and T_m. Here, infl./cross. point, inflection or crossing point.

ical order of amorphous Gd-Co thin films using the extended x-ray absorption fine structure (EXAFS) and x-ray photoelectron spectroscopy (XPS) methods. The high sensitivity of the methods allowed the small contribution of RE oxide to be detected, while TM oxidization was not revealed by the analysis. Similar results were obtained by Haltz *et al.* for TbFe alloys [20]. This indicates that the element concentration profile naturally occurs in the RE-TM nanosystems even when they are protected by capping layers. While the concentration profile of TM atoms can be considered as approximately constant, a deficit of RE atoms with a nominal magnetic moment is expected near the surface. Additionally, RE-TM systems are susceptible to aging processes caused by the high affinity of RE elements for oxygen [2], which slowly reduces the proportion of the nonoxidized RE atoms at the surface. Only the middle part of a thin layer or nanoparticle is expected to be a bulklike alloy with an almost nominal effective composition that does not change significantly over time.

To analyze the preferential oxidation process, we assumed that oxygen atoms bond only with rare earth atoms, change their magnetic moment, and switch them off magnetically. Therefore we accepted a constant concentration profile of Fe atoms in the entire volume of the nanoparticle and a Gaussian distribution of magnetic nonoxidized Tb content as a function of the radius, shown in Fig. 5(a). The width σ of the distribution was varied from 0.5 to 5.0 of the normalized radius. The smallest width of the distribution yields a more than five times reduction in the concentration of nonoxidized Tb atoms on the surface of the nanoparticle, while the latter value corresponds to the negligible oxidation of rare earth atoms. The composition of the alloy in the center of the nanoparticle was always kept as nominal. A similar approach can also be adopted for thin films, but instead of the radius, the layer thickness is taken as an independent variable in the terbium content distribution.

Since the magnetic properties of ferrimagnetic alloys are highly sensitive to rare earth content, a small decline in nonoxidized Tb can significantly alter the net magnetization and its behavior versus temperature. Figure 5(b) presents the calculated $M_R(T)$ curves for a particle with a diameter of 10 nm, and qualitatively the same results were obtained for systems of different sizes (Supplemental Material, Figs. S4 and S5 [42]) as well as for thin films with thicknesses of 5, 10, and 15 nm (Supplemental Material, Figs. S6– S8 [42]). The oxidation directly influences the compensation temperature, as shown in Fig. 5(c). The values depicted in the graph have been determined using two methods: by the minimum of susceptibility and by the intersection of the $M_R(T)$ curve with the axis $M_R = 0$. The two approaches give very similar results, differing from each other only by a few kelvins. The differences are greater only in the case of the smallest nanoparticles due to the statistical fluctuations. The reduction of the compensation temperature is directly caused by the change in the average alloy composition towards an Fe-rich system, and for $\sigma < 1$

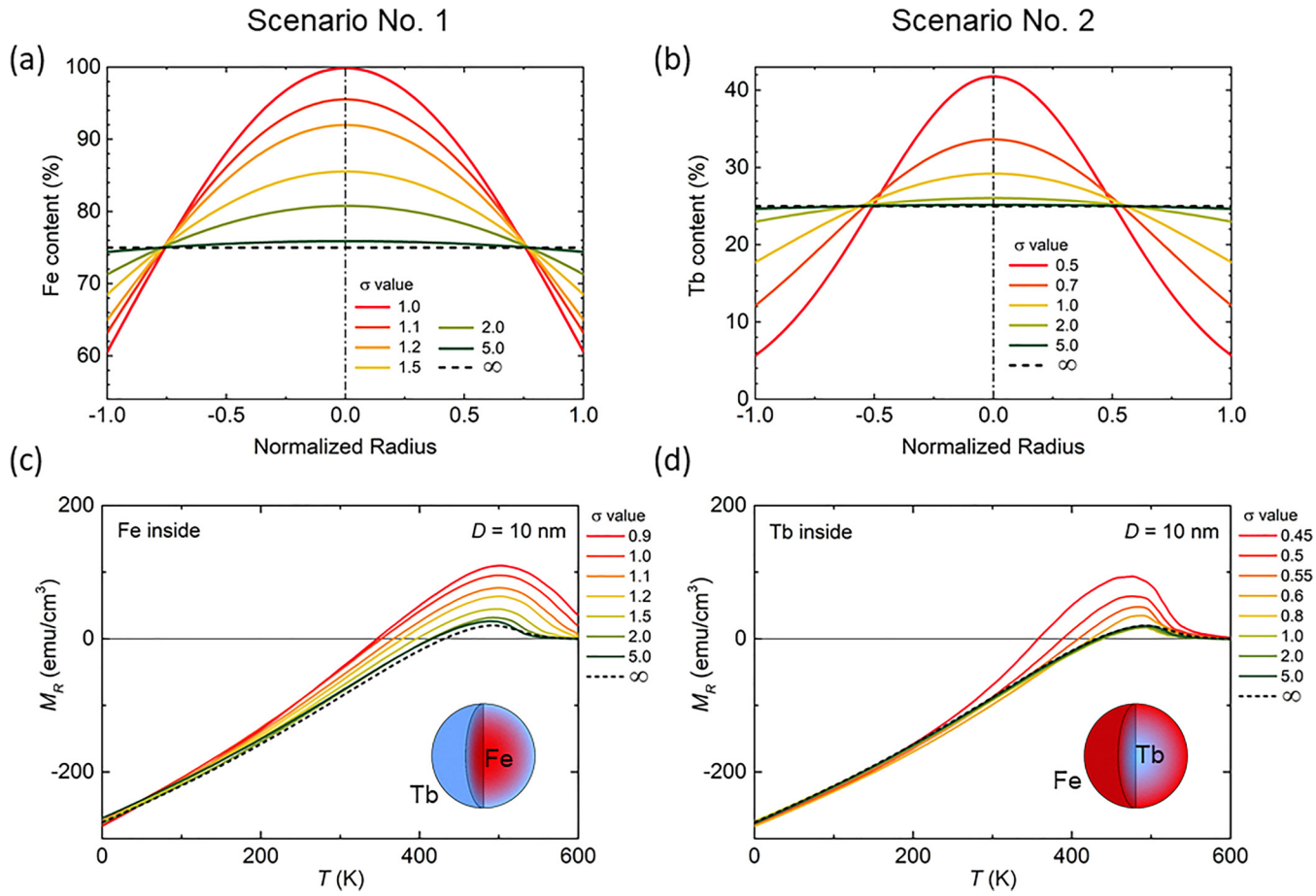

FIG. 6. (a) and (b) Distributions of Fe and Tb content in a nanoparticle as a function of distance from its center. The widths of the distributions are expressed in the normalized radius of the nanoparticle. The infinite-sigma value corresponds to a homogeneous concentration distribution throughout the volume of the nanoparticle. (c) and (d) Remanent magnetization vs temperature for a 10-nm nanoparticle with various distributions of terbium and iron content.

the nanoparticle becomes a TM-dominant alloy in the entire temperature range. Qualitatively the same transition was reported by Hebler *et al.* [12] as a function of the TbFe alloy thickness, which suggests that preferential oxidation plays a key role in layers thinner than 20 nm and significantly influences their magnetic properties. The changes are accompanied by a shift in the Curie temperature [Fig. 5(c)] resulting from the reduced effective magnetic coupling between the RE and TM atoms caused by a smaller number of atoms interacting within their first coordination shell. Our calculations for thin films (Supplemental Material, Fig. S9 [42]) seem to confirm these findings, where a qualitatively similar behavior to that found for nanoparticles was revealed. However, the trend of T_C and T_m is described by a function with a slightly different profile, which shows that a clear change in the Curie and compensation temperatures can be expected in thin films only at a sufficiently high oxidation rate ($\sigma < 2$).

C. Chemical segregation

RE-TM amorphous alloys are metastable, and their structures undergo continuous atomic rearrangement [2,39,43]. This results in microscopic inhomogeneities and compositional variability along the film-normal direction [17,38]. For example, Haltz *et al.* demonstrated that the surface of the Tb-Fe thin layer is richer in Tb, depleting the bulklike part [20]. Partial phase separation and segregation has been observed in the same alloys also by Heigl *et al.* [44]. Nonuniform contrast in the other RE-TM films along the thickness direction has been reported by other authors as well [18,19,23,45]. The local variations of alloy composition according to published analyses can reach 10–20% relative to the mean, but some authors suggest [43] that the maximum deviation may actually be larger because the local chemical techniques average a signal over an area that can be bigger than the fluctuation length scale.

Since the progress of the atomic segregation in RE-TM alloys is not yet well understood, and the reports on it are rare and not completely consistent with each other, we assumed two segregation scenarios. The first is to consider terbium as a surfactant and assume its segregation to the surface, while in the second scenario Tb atoms segregate to the center of the nanoparticle. The concentration distributions of atoms were assumed to be Gaussian, as shown in Figs. 6(a) and 6(b). In each case, the content of the second element was assumed to be such that the alloy composition averaged over the volume of the nanoparticle was nominal and amounted to 25 at. % Tb and 75 at. % Fe. A similar approach can be applied to

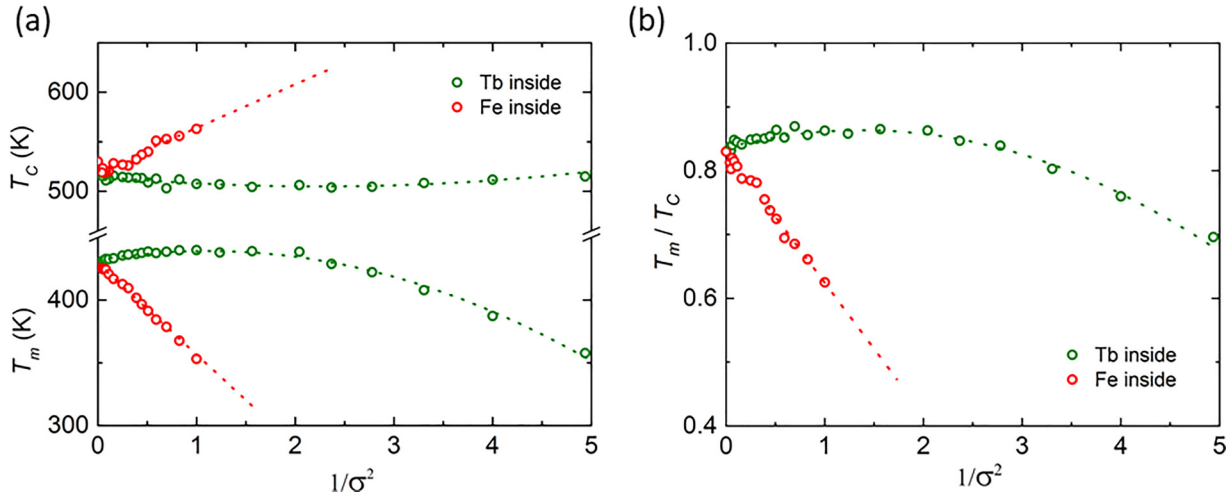

FIG. 7. (a) Compensation and Curie temperatures determined for 10-nm nanoparticles for two scenarios: Tb atoms segregating to the surface (open red circles) and Tb atoms segregating to the center of a nanoparticle (open green circles). (b) Ratio of compensation temperature to Curie temperature for two segregation scenarios. σ is the width of concentration distributions as defined in Fig. 6.

thin layers; however, in this case the independent variable for element content distributions is the normalized layer thickness (Supplemental Material, Figs. S10 and S11 [42]). The outcome of atomistic simulations presenting the remanence curves as a function of temperature is shown in Figs. 6(c) and 6(d) for nanoparticles and in the Supplemental Material, Fig. S12 [42], for thin films. Surprisingly, regardless of the assumed scenario, the obtained results are qualitatively consistent with each other. In each case, increasing the degree of chemical segregation results in a general trend of decreasing the compensation temperature and increasing the Curie temperature. The latter effect can be associated with the appearance of an almost pure iron phase, which has a Curie temperature of 1043 K, much higher than the Curie temperature of the considered TbFe alloy. Simultaneously, changes in the compensation temperature are observed and can be associated with a reduction of the effective antiferromagnetic coupling between the RE and TM atoms caused by there being a reduced number of atoms that can interact with atoms of different species [2,46]. The greater the segregation, the smaller the antiferromagnetic interaction between the RE and TM atoms, which causes a decrease in the width of the fanning cone for the Tb and Fe moments. The Fe fanning cone declines faster due to the higher iron content in the system and the easier formation of the almost pure iron phase. This is observed both as a decrease in the compensation temperature and as an increase in the remanence of the Fe-rich region above the compensation temperature. Signatures of such an influence of nanoscale composition inhomogeneities and chemical segregation on the compensation temperature were noted also by Liu *et al.* [47] in TbFeCo amorphous alloys.

Closer analysis shows that the modification of the magnetic properties depends quantitatively on the type of segregation, which is visible in Fig. 7. When iron migrates to the center of the nanoparticle, the compensation temperature decreases linearly with the square of the reciprocal of the concentration distribution width. However, when terbium migrates inside, this relationship is quadratic, and even a slight increase in the compensation temperature is observed for a small degree of segregation [Fig. 7(a)]. As a result, the ratio T_m/T_C drops sharply and linearly as Tb diffuses to the surface. In contrast, when Fe is a surfactant, the ratio T_m/T_C changes only slightly, at least for a small degree of segregation [Fig. 7(b)]. This gives us the opportunity to experimentally determine which scenario is present in the system and track its course. The full explanation of the occurrence of such relationships is not entirely clear; however, it seems that they are universal for spherical objects and occur for any size of nanoparticles (Supplemental Material, Figs. S13 and S14 [42]). Our calculations also predict qualitatively similar behavior of the compensation temperature and Curie temperature in thin films; however, due to the different geometry of the system, the shape of T_m/T_C curves is slightly different (Supplemental Material, Fig. S15 [42]). Since chemical segregation can be triggered or accelerated by temperature, this effect can be used for tailoring the systems with designed magnetization and compensation temperature by controlled heating. On the other hand, the occurrence of this effect indicates that RE-TM alloys may slowly change their properties with time when progressive segregation occurs, in particular when the alloys are incidentally subjected to elevated temperatures. This may affect their possible applications as materials for spintronic devices or information recording and processing.

IV. CONCLUSIONS

In conclusion, we have studied three surface effects for representative amorphous ferrimagnetic TbFe nanoparticles and thin films of various diameters and thicknesses with 25 at. % Tb. We have shown that the reduction of the average number of neighbors on the surface is significant only for nanosystems with a size of a few nanometers and cannot alone explain the large changes in compensation temperature observed in thin metal layers as a function of their thickness. The latter, on the other hand, can be explained by preferential oxidation, which may partially occur even when the alloy is covered

with a protective layer. Our results suggest that the preferential oxidation plays a key role even for systems containing a very low concentration of oxygen, which significantly influences their magnetic properties. Our results point also to the importance of chemical segregation. We have shown that regardless of its character, a general trend of decreasing the compensation temperature and increasing the Curie temperature can be expected. Simultaneously, an increase in the net magnetic moment at temperatures above T_m is observed in comparison with perfectly alloyed, nonsegregated systems. Although the segregation seems to be easy to control using heating protocols, its occurrence can cause slowly progressing changes in the material, which is disadvantageous from the application point of view. On the other hand, the ability to fine-tune the compensation temperature by means of surface effects suggests that this approach could be used to advantage. For example, the most effective all-optical switching occurs near the compensation temperature, which means that the concentration range of RE-TM alloys accessible for the switching can be extended using nanopatterning methods or controlled thermal treating initiating chemical segregation.

The magnitudes of all of the studied surface effects are measurable and significant for all types of nanosystems (nanoparticles, thin films, and patterned layers); therefore they must be taken into account in order to obtain quantitative agreement between magnetic simulations and experimental outcomes. Our results also suggest an experimental way to verify which of the processes plays a leading role in a given system. Such experimental verification is possible, in particular, by measuring the temperature ratio T_m/T_C as a function of the characteristic size of the system, as this parameter behaves in a significantly different way depending on the considered surface effect.

ACKNOWLEDGMENTS

We thank Sergiu Ruta of Sheffield Hallam University and Nguyen Thanh Binh of the University of York for insightful remarks and discussions. We gratefully acknowledge the Polish high-performance computing infrastructure PLGrid (HPC Centers: ACK Cyfronet AGH) for providing computer facilities and support within computational Grant No. PLG/2021/015143.

[1] A. Chanda, J. E. Shoup, N. Schulz, D. A. Arena, and H. Srikanth, Tunable competing magnetic anisotropies and spin reconfigurations in ferrimagnetic $Fe_{100-x}Gd_x$ alloy films, Phys. Rev. B **104**, 094404 (2021).

[2] G. Sala, C.-H. Lambert, S. Finizio, V. Raposo, V. Krizakova, G. Krishnaswamy, M. Weigand, J. Raabe, M. D. Rossell, E. Martinez, and P. Gambardella, Asynchronous current-induced switching of rare-earth and transition-metal sublattices in ferrimagnetic alloys, Nat. Mater. **21**, 640 (2022).

[3] A. Hernando, C. Prados, and C. Prieto, Anisotropy, magnetostriction and local chemical order in amorphous $Tb_xFe_{1-x}(0.1 < x < 0.55)$ thin films, J. Magn. Magn. Mater. **157-158**, 501 (1996).

[4] A. Ceballos, A. Pattabi, A. El-Ghazaly, S. Ruta, C. P. Simon, R. F. L. Evans, T. Ostler, R. W. Chantrell, E. Kennedy, M. Scott, J. Bokor, and F. Hellman, Role of element-specific damping in ultrafast, helicity-independent, all-optical switching dynamics in amorphous (Gd,Tb)Co thin films, Phys. Rev. B **103**, 024438 (2021).

[5] Ł. Frąckowiak, P. Kuświk, G. D. Chaves-O'Flynn, M. Urbaniak, M. Matczak, P. P. Michałowski, A. Maziewski, M. Reginka, A. Ehresmann, and F. Stobiecki, Magnetic domains without domain walls: A unique effect of He^+ ion bombardment in ferrimagnetic Tb/Co films, Phys. Rev. Lett. **124**, 047203 (2020).

[6] Ł. Frąckowiak, F. Stobiecki, M. Urbaniak, M. Matczak, G. D. Chaves-O'Flynn, M. Bilski, A. Glenz, and P. Kuświk, Magnetic properties of Co-Tb alloy films and Tb/Co multilayers as a function of concentration and thickness, J. Magn. Magn. Mater. **544**, 168682 (2022).

[7] J. Finley and L. Liu, Spin-orbit-torque efficiency in compensated ferrimagnetic cobalt-terbium alloys, Phys. Rev. Appl. **6**, 054001 (2016).

[8] R. Basumatary, P. Behera, B. Basumatary, B. Brahma, S. Ravi, R. Brahma, and S. Srivastava, Influence of surface roughness on magnetic properties of CoTbNi ternary alloy films, Micro Nanostruct. **174**, 207491 (2023).

[9] A. Talapatra, J. A. Chelvane, and J. Mohanty, Tuning magnetic microstructure in Gd-Fe thin films: Experiment and simulation, J. Magn. Magn. Mater. **448**, 360 (2018).

[10] M. Krupinski, J. Hintermayr, P. Sobieszczyk, and M. Albrecht, Control of magnetic properties in ferrimagnetic GdFe and TbFe thin films by He^+ and Ne^+ irradiation, Phys. Rev. Mater. **5**, 024405 (2021).

[11] M. Ishibashi, K. Yakushiji, M. Kawaguchi, A. Tsukamoto, S. Nakatsuji, and M. Hayashi, Ferrimagnetic compensation and its thickness dependence in TbFeCo alloy thin films, Appl. Phys. Lett. **120**, 022405 (2022).

[12] B. Hebler, A. Hassdenteufel, P. Reinhardt, H. Karl, and M. Albrecht, Ferrimagnetic Tb–Fe alloy thin films: Composition and thickness dependence of magnetic properties and all-optical switching, Front. Mater. **3**, 8 (2016).

[13] R. Malmhäll and T. Chen, Thickness dependence of magnetic hysteretic properties of rf-sputtered amorphous Tb-Fe alloy thin films, J. Appl. Phys. **53**, 7843 (1982).

[14] R. J. Gambino and J. J. Cuomo, Selective resputtering-induced anisotropy in amorphous films, J. Vac. Sci. Technol. **15**, 296 (1978).

[15] V. G. Harris, K. D. Aylesworth, B. N. Das, W. T. Elam, and N. C. Koon, Structural origins of magnetic anisotropy in sputtered amorphous Tb-Fe films, Phys. Rev. Lett. **69**, 1939 (1992).

[16] M. Kim, J. Bow, R. Carpenter, J. Liu, S. G. Kim, S. K. Lee, W. M. Kim, and J. S. Yoon, Nanostructure and chemical inhomogeneity in TbFe magneto-optical films, IEEE Trans. Magn. **30**, 4398 (1994).

[17] T. Gao, X. Xu, S. Zhou, J. Li, A.-L. Xia, and B.-S. Han, Phase segregation and exchange biasing in TbFeCo films with perpendicular anisotropy, J. Magn. Magn. Mater. **306**, 324 (2006).

[18] D.-H. Kim, M. Haruta, H.-W. Ko, G. Go, H.-J. Park, T. Nishimura, D.-Y. Kim, T. Okuno, Y. Hirata, Y. Futakawa, H. Yoshikawa, W. Ham, S. Kim, H. Kurata, A. Tsukamoto, Y. Shiota, T. Moriyama, S.-B. Choe, K.-J. Lee, and T. Ono, Bulk Dzyaloshinskii–Moriya interaction in amorphous ferrimagnetic alloys, Nat. Mater. **18**, 685 (2019).

[19] S. Krishnia, E. Haltz, L. Berges, L. Aballe, M. Foerster, L. Bocher, R. Weil, A. Thiaville, J. Sampaio, and A. Mougin, Spin-orbit coupling in single-layer ferrimagnets: Direct observation of spin-orbit torques and chiral spin textures, Phys. Rev. Appl. **16**, 024040 (2021).

[20] E. Haltz, R. Weil, J. Sampaio, A. Pointillon, O. Rousseau, K. March, N. Brun, Z. Li, E. Briand, C. Bachelet, Y. Dumont, and A. Mougin, Deviations from bulk behavior in TbFe(Co) thin films: Interfaces contribution in the biased composition, Phys. Rev. Mater. **2**, 104410 (2018).

[21] K. Wang, S. Dong, and Z. Xu, Thickness and substrate effects on the perpendicular magnetic properties of ultra-thin TbFeCo films, Surf. Coat. Technol. **359**, 296 (2019).

[22] K. Ueda, A. J. Tan, and G. S. D. Beach, Effect of annealing on magnetic properties in ferrimagnetic GdCo alloy films with bulk perpendicular magnetic anisotropy, AIP Adv. **8**, 125204 (2018).

[23] N. Bergeard, A. Mougin, M. Izquierdo, E. Fonda, and F. Sirotti, Correlation between structure, electronic properties, and magnetism in Co_xGd_{1-x} thin amorphous films, Phys. Rev. B **96**, 064418 (2017).

[24] A. Talapatra, J. A. Chelvane, B. Satpati, S. Kumar, and J. Mohanty, Tunable magnetic domains and depth resolved microstructure in Gd-Fe thin films, J. Alloys Compd. **774**, 1059 (2019).

[25] S. Mondal, A. Talapatra, J. Chelvane, J. R. Mohanty, and A. Barman, Role of magnetic anisotropy in the ultrafast magnetization dynamics of Gd-Fe thin films of different thicknesses, Phys. Rev. B **100**, 054436 (2019).

[26] C. T. Ma, B. J. Kirby, X. Li, and S. J. Poon, Thickness dependence of ferrimagnetic compensation in amorphous rare-earth transition-metal thin films, Appl. Phys. Lett. **113**, 172404 (2018).

[27] H. Takagi, S. Tsunashima, S. Uchiyama, and T. Fujii, Stress induced anisotropy in amorphous Gd-Fe and Tb-Fe sputtered films, J. Appl. Phys. **50**, 1642 (1979).

[28] T. Ruckert, J. Tappert, R. Brand, and W. Keune, Mössbauer-effect study of amorphous $Tb_{1-x}Fe_x$ films, J. Magn. Magn. Mater. **165**, 411 (1997).

[29] P. Si, E. Brück, Z. Zhang, O. Tegus, K. Buschow, W. Zhang, J. Klaasse, and F. de Boer, Synthesis, structure and magnetic properties of Fe–Gd nanocapsules coated with B_2O_3/H_3BO_3 and $Fe_3BO_5 + GdBO_3$, Phys. B (Amsterdam) **353**, 1 (2004).

[30] S. P. Singh, R. Witte, O. Clemens, A. Sarkar, L. Velasco, R. Kruk, and H. Hahn, Magnetic $Tb_{75}Fe_{25}$ nanoglass for cryogenic permanent magnet undulator, ACS Appl. Nano Mater. **3**, 7281 (2020).

[31] R. F. L. Evans, W. J. Fan, P. Chureemart, T. A. Ostler, M. O. A. Ellis, and R. W. Chantrell, Atomistic spin model simulations of magnetic nanomaterials, J. Phys.: Condens. Matter **26**, 103202 (2014).

[32] T. A. Ostler, R. F. L. Evans, R. W. Chantrell, U. Atxitia, O. Chubykalo-Fesenko, I. Radu, R. Abrudan, F. Radu, A. Tsukamoto, A. Itoh, A. Kirilyuk, T. Rasing, and A. Kimel, Crystallographically amorphous ferrimagnetic alloys: Comparing a localized atomistic spin model with experiments, Phys. Rev. B **84**, 024407 (2011).

[33] J. L. García-Palacios and F. J. Lázaro, Langevin-dynamics study of the dynamical properties of small magnetic particles, Phys. Rev. B **58**, 14937 (1998).

[34] P. Hansen, C. Clausen, G. Much, M. Rosenkranz, and K. Witter, Magnetic and magneto-optical properties of rare-earth transition-metal alloys containing Gd, Tb, Fe, Co, J. Appl. Phys. **66**, 756 (1989).

[35] X. Jiao, Z. Zhang, and Y. Liu, Modeling of temperature dependence of magnetization in TbFe films — An atomistic spin simulation study, SPIN **06**, 1650003 (2016).

[36] I. Radu, K. Vahaplar, C. Stamm, T. Kachel, N. Pontius, H. A. Dürr, T. A. Ostler, J. Barker, R. F. L. Evans, R. W. Chantrell, A. Tsukamoto, A. Itoh, A. Kirilyuk, T. Rasing, and A. V. Kimel, Transient ferromagnetic-like state mediating ultrafast reversal of antiferromagnetically coupled spins, Nature (London) **472**, 205 (2011).

[37] D. A. Garanin, Self-consistent Gaussian approximation for classical spin systems: Thermodynamics, Phys. Rev. B **53**, 11593 (1996).

[38] E. Kirk, C. Bull, S. Finizio, H. Sepehri-Amin, S. Wintz, A. K. Suszka, N. S. Bingham, P. Warnicke, K. Hono, P. W. Nutter, J. Raabe, G. Hrkac, T. Thomson, and L. J. Heyderman, Anisotropy-induced spin reorientation in chemically modulated amorphous ferrimagnetic films, Phys. Rev. Mater. **4**, 074403 (2020).

[39] G. Sala and P. Gambardella, Ferrimagnetic dynamics induced by spin-orbit torques, Adv. Mater. Interfaces **9**, 2201622 (2022).

[40] D. Chen, Y. Xu, S. Tong, W. Zheng, Y. Sun, J. Lu, N. Lei, D. Wei, and J. Zhao, Noncollinear spin state and unusual magnetoresistance in ferrimagnet Co-Gd, Phys. Rev. Mater. **6**, 014402 (2022).

[41] C. Schubert, Thin amorphous Fe-Tb alloy films, in *Magnetic Order and Coupling Phenomena: A Study of Magnetic Structure and Magnetization Reversal Processes in Rare-Earth–Transition-Metal Based Alloys and Heterostructures*, Springer Theses (Springer, New York, 2014), pp. 5–17.

[42] See Supplemental Material at http://link.aps.org/supplemental/10.1103/PhysRevB.109.024412 for additional results for nanoparticles with different diameters and results for thin films.

[43] P. Hansen, Magnetic amorphous alloys, in *Handbook of Magnetic Materials* (Elsevier, New York, 1991), Chap. 4, pp. 289–452.

[44] M. Heigl, C. Mangkornkarn, A. Ullrich, M. Krupinski, and M. Albrecht, Enhanced annealing stability of ferrimagnetic Tb/FeCo multilayers, AIP Adv. **11**, 085112 (2021).

[45] C. E. Graves, A. H. Reid, T. Wang, B. Wu, S. de Jong, K. Vahaplar, I. Radu, D. P. Bernstein, M. Messerschmidt, L. Müller, R. Coffee, M. Bionta, S. W. Epp, R. Hartmann, N. Kimmel, G. Hauser, A. Hartmann, P. Holl, H. Gorke, J. H. Mentink *et al.*, Nanoscale spin reversal by non-local angular momentum transfer following ultrafast laser

excitation in ferrimagnetic GdFeCo, Nat. Mater. **12**, 293 (2013).

[46] N. R. Anderson and R. E. Camley, Temperature-dependent magnetization in bimagnetic nanoparticles with antiferromagnetic interfacial exchange, Phys. Rev. B **94**, 134432 (2016).

[47] T.-M. Liu, T. Wang, A. H. Reid, M. Savoini, X. Wu, B. Koene, P. Granitzka, C. E. Graves, D. J. Higley, Z. Chen, G. Razinskas, M. Hantschmann, A. Scherz, J. Stöhr, A. Tsukamoto, B. Hecht, A. V. Kimel, A. Kirilyuk, T. Rasing, and H. A. Dürr, Nanoscale confinement of all-optical magnetic switching in TbFeCo - competition with nanoscale heterogeneity, Nano Lett. **15**, 6862 (2015).